Applied Physics Letters

Realizing Anderson localization of surface plasmon polaritons and enhancing their interactions with excitons in 2D disordered nanostructures

Cite as: Appl. Phys. Lett. **116**, 201106 (2020); https://doi.org/10.1063/5.0001451
Submitted: 18 January 2020 . Accepted: 04 May 2020 . Published Online: 19 May 2020

Yingying Zhu, Hao Jing, Ru-Wen Peng, Cheng-Yao Li, Jie He, Bo Xiong, and Mu Wang

AIP Publishing

Applied Physics Letters ARTICLE scitation.org/journal/apl

Realizing Anderson localization of surface plasmon polaritons and enhancing their interactions with excitons in 2D disordered nanostructures

Cite as: Appl. Phys. Lett. **116**, 201106 (2020); doi: 10.1063/5.0001451
Submitted: 18 January 2020 · Accepted: 4 May 2020 ·
Published Online: 19 May 2020

Yingying Zhu, Hao Jing, Ru-Wen Peng,[a] Cheng-Yao Li, Jie He, Bo Xiong, and Mu Wang[a]

AFFILIATIONS

National Laboratory of Solid State Microstructures, School of Physics, and Collaborative Innovation Center of Advanced Microstructures, Nanjing University, Nanjing 210093, China

[a]Authors to whom correspondence should be addressed: rwpeng@nju.edu.cn and muwang@nju.edu.cn

ABSTRACT

Surface plasmon polaritons (SPPs) propagating on a metal–dielectric interface suffer from inevitable energy losses originating from metals, especially in a visible regime, which degrades the quality of SPP-based devices. However, if the size of the devices is sufficiently miniaturized, we can thereby limit the propagation length of the signals and effectively circumvent the problems of large propagation losses. Anderson localization is a possible approach to squeeze SPPs. In this Letter, we experimentally demonstrate the Anderson localization of SPPs at optical frequencies in two-dimensional (2D) nanostructures. By increasing the positional disorder of the silver nanohole arrays on a glass substrate, strong 2D localization of SPPs appears with an exponentially decreased electric field, reduced propagation length, and the rapid disappearance of the autocorrelation coefficient. Moreover, we manage to realize the localized SPP-exciton interactions in the 2D disordered silver nanoarrays combined with fluorescent dye molecules. Due to the disorder in the nanoarray, the collected photoluminescence from fluorescent dye molecules is enhanced by over three orders of magnitude compared to that on the silver film without nanostructures. Our study extends Anderson localization of SPPs at the visible regime to 2D disordered systems and provides a unique way to enhance light–matter interaction in SPP-based nanodevices.

Surface plasmon polaritons (SPPs) are transverse magnetic (TM)-polarized optical surface waves that propagate along a metal–dielectric interface,[1] which provide a possible solution for confined light at a sub-wavelength scale and stimulate strong light-matter interactions.[1–4] These properties of SPPs are useful for fields such as photodetectors,[5,6] spectroscopies,[7] lasers,[8–10] photocatalysis,[11] nonlinear optics,[12] and solar cells.[13] To improve practical performances, tailoring the in-plane propagation of SPPs is essential. Such manipulations can be realized by integrating SPPs with sub-wavelength elements such as nanoparticles,[14] nanowires,[15] and metasurfaces,[16] or by altering the properties of the material through phase transitions,[17] or electrostatic gating.[18,19] However, when SPP waves propagate along the interface between metal and dielectric materials, they undergo high energy losses, especially at visible wavelengths. This constrains the functionality of SPP-based devices. However, the drawback of large propagation losses can be circumvented by shortening the propagation length of SPP waves. A possible approach to squeeze SPPs is Anderson localization.

Anderson localization of light waves has become the forefront of research over the past decade.[20–25] Direct observations of Anderson localization have been successfully made in disordered photonic lattices[26–29] or coupled waveguide arrays,[30,31] stimulating applications in imaging,[32] random lasing,[33,34] absorbers,[35] and so on. To effectively utilize SPPs, the realization of Anderson localization of SPPs can scale down the size of devices, which inherently reduce energy losses caused by metals. More importantly, it can associate spatial-disorder-induced light localization with SPP-induced light confinement. Therefore, significantly strong light–matter interactions can be achieved. Very recently, Anderson localization of SPPs with one-dimensional (1D) engineered disorder has been experimentally observed in the visible range.[36] However, 1D Anderson localization of SPPs provides light confinement only in one direction, which lacks the modulated level of functionality for most SPP-based nanodevices.

In this Letter, we experimentally demonstrate the Anderson localization of SPPs in the visible regime in 2D nanostructures with the engineered disorder and show the enhancement of their

interactions with excitons when the disordered nanostructure combines with fluorescent dye molecules. It is shown that with increasing the positional disorder of the silver nanohole arrays on a glass substrate, strong 2D localization of SPPs appears with the exponentially decreased electric field, reduced propagation length, and rapid disappearance of the autocorrelation coefficient. Furthermore, by combining the disordered nanoarrays with fluorescent dye molecules (i.e., IR-140 dye molecules), we realize the enhanced SPP-exciton interactions. It is found that the collected photoluminescence (PL) intensity from dye molecules is increased by over three orders of magnitude compared to that on the silver film without nanostructures. Our results extend the Anderson localization of SPPs in the visible regime to 2D disordered systems and may foreshadow other opportunities in extremely enhanced light–matter interactions by relying on SPP-based devices.

The nanostructures we studied are composed of a 2D array of etched nanoholes in the 100-nm-thick silver surface on a glass substrate, as illustrated in Fig. 1(a). To observe the effect of Anderson localization, we gradually perturb the position of each component in the square nanoarray while preserving the radius of each hole. The disorder degree of the nanoarray can be defined as $\eta = \Delta\mathbf{r}/p$, where p is the array period and $\Delta\mathbf{r} = \Delta\mathbf{x} + \Delta\mathbf{y}$ is the random position deviation of each hole from the periodic array. In Fig. 1(a), the nanoarrays of $\eta = 0\%$, 20%, 40%, and 60% are visualized with $p = 1.5\ \mu$m and nanohole radius $r = 300$ nm. We first apply the full-wave finite-difference time-domain (FDTD) method to simulate the propagation of SPPs in different nanostructures. In the simulations, we employ a Gaussian beam (waist radius of 1 μm and x-span of 6 μm) with the wavelength $\lambda = 655$ nm to illuminate an in-coupling slit, which has a length of 15 μm and a width of 0.2 μm. Then, the SPPs are excited in the slit and propagate along the y-direction. Eventually, the SPP beams with the x-span of around 6.5 μm reach the nanohole array (15 μm × 15 μm), and the central position of these launched beams is indicated by the red arrow in Fig. 1(a). The corresponding electric-field distribution at the Ag–glass interface of the nanostructure has been calculated and is shown in Fig. 1(b), with an increased disorder degree. From the simulation results, we find that the spatial spreading of the field distribution shrinks when increasing disorder degree, and there is a monotonic decrease in the SPP propagation length. The simulated electric-field distributions in the nanoarrays are plotted along the x- and y-directions in Figs. 1(c) and 1(d), which are taken along the white dashed lines in Fig. 1(b). In the periodic nanoarray ($\eta = 0\%$), the electric-field distribution shows a symmetric extended pattern along the x-direction and an evident propagation feature along the y-direction. However, when the disorder degree increases, the field exponentially decreases, followed by an enhancement of the local field intensity. The main intensity peak of the simulated electric-field is enhanced approximately twice in the disordered structure ($\eta = 60\%$) compared to the periodic structure ($\eta = 0\%$). The above results reveal that the localization of SPPs occurs in 2D plasmonic nanostructures, with the increased positional disorder.

We then identify the strong localization of the SPPs with quantities such as an effective propagation length and autocorrelation coefficient based on the simulation results. First, the standard quantity used to describe the phenomenon of Anderson localization is the inverse participation ratio $P = \int I^2(x)dx / \{\int I(x)dx\}^2$,[37] where $I(x)$ is the integrated field intensity in the y-direction. The effective propagation length is defined as $L_{eff} = P^{-1}$. The calculated P and L_{eff} values were averaged over 15 structures with different nanohole arrangements and are shown in Figs. 2(a) and 2(b) with varying disorder degrees. The inverse

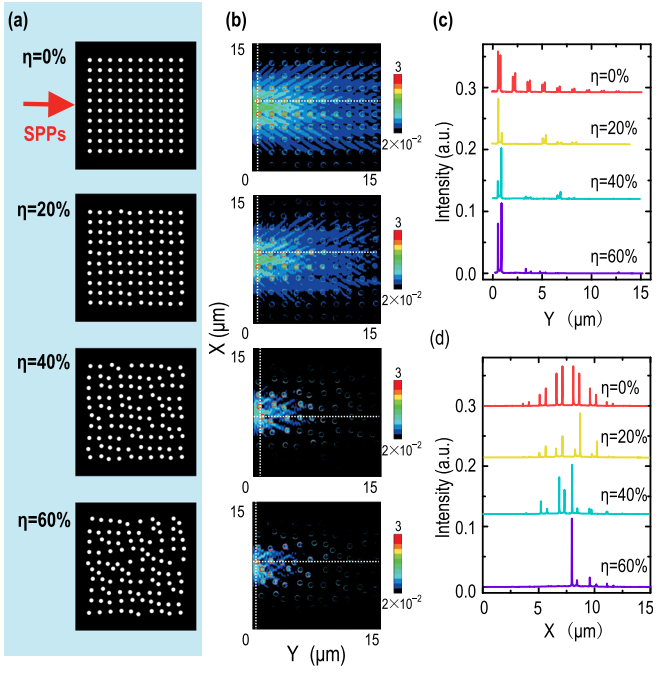

FIG. 1. (a) Illustration of nanohole array patterns on the silver surface. Disorder degree $\eta = 0\%$, 20%, 40%, and 60%, from top to bottom. SPPs are launched at the location marked by the red arrow. (b) Calculated electric-field distributions at the Ag–glass interface of the nanohole arrays with different disorder degrees, corresponding to (a). (c) and (d) Calculated electric-field intensity along the white dashed lines in (b) with increasing disorder degree. Each subplot is plotted at the same scaling.

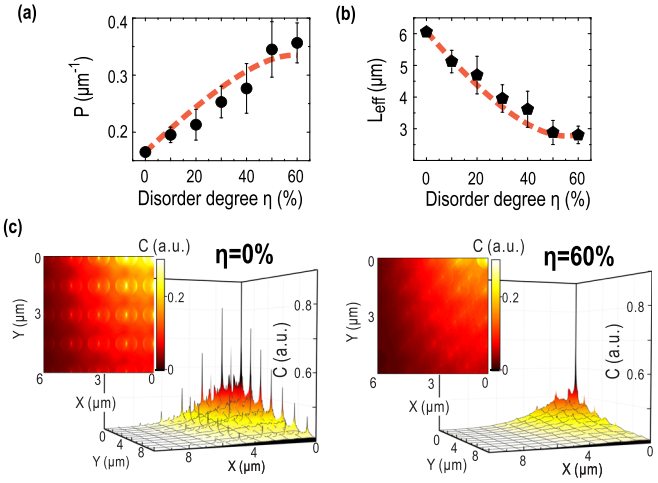

FIG. 2. (a) Calculated inverse participation ratio P and (b) effective propagation length L_{eff} as a function of disorder degree. Both values were averaged over 15 structures with different nanohole arrangements. (c) 2D color maps (inset) and 3D color maps of the autocorrelation function of the calculated electric-field distributions, for samples with the disorder degree $\eta = 0\%$ and $\eta = 60\%$, respectively.

participation ratio increases, while the effective propagation length decreases, with increasing disorder degree. Both tend to converge at higher disorder degrees. This result demonstrates that the confinement of SPP propagation is due to disorder. Second, we apply the autocorrelation function on the calculated electric field distributions of the designed nanostructures in Fig. 1(a) with different disorder degrees as[38,39]

$$C(x,y) = \int f(x,y) \cdot f^*(\xi + x, \varsigma + y) d\xi d\varsigma, \quad (1)$$

where $f(x,y)$ is the electric-field intensity. Figure 2(c) shows the 2D color maps (inset) and 3D color maps of the calculated autocorrelation functions with disorder degrees of $\eta = 0\%$ and $\eta = 60\%$. For the periodic nanoarray ($\eta = 0\%$), the value of $C(x,y)$ oscillates and gradually decreases from its initial value $C(0,0) = 1$. However, when increasing the level of disorder degree $\eta = 60\%$, $C(x,y)$ dramatically drops to zero along both the x- and y-directions. The autocorrelation results further demonstrate that the short-range disorder gives rise to the disappearance of autocorrelation and, hence, causes the Anderson localization of the SPPs.

We further clarify the underlying mechanism of the Anderson localization of SPPs based on the simulations. The Fourier transformation (FT) method is applied to the calculated electric-field distributions. The information in Fourier space gives direct access to the different SPP wave vectors that constitute the field.[40] The FT of the calculated electric-field distributions in our 2D nanohole arrays, with the disorder degree, increased from $\eta = 0\%$ to $\eta = 60\%$ are shown in Fig. 3. The wave vectors have been normalized by the SPP wave vector at a flat Ag layer on the glass substrate. From Fig. 3, we found that the FT retains periodic peaks in the k_x–k_y plane for the periodic nanostructure, while only zero- and first-order peaks remain for $\eta = 60\%$. These features indicate that more SPP wave vectors are generated in the disordered nanoarrays. This phenomenon originates from the stronger multiple scattering among the nanoholes, and their collective effect eventually leads to SPP localization.

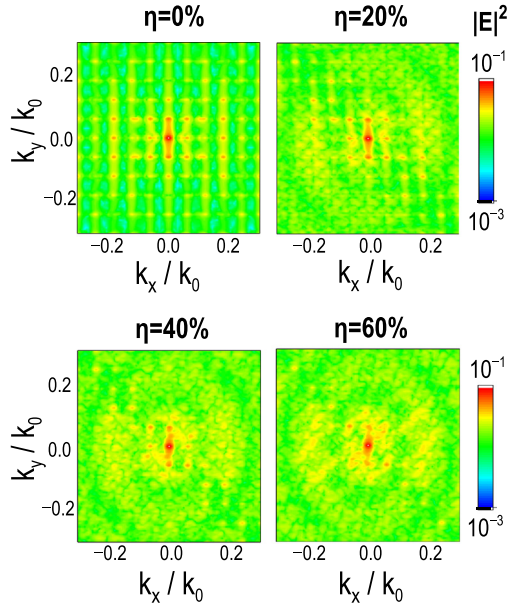

FIG. 3. Fourier transformation of the calculated electric-field distributions in the nanohole arrays with different disorder degrees.

Experimentally, we fabricated the samples using the designed layouts according to Fig. 1(a). A 100-nm-thick silver layer was deposited by magnetron sputtering on a glass substrate. Then, the nanohole arrays were etched using the focused ion beam (Helios Nanolab 600i) technique. As shown in Fig. 4(a), in-coupling and out-coupling slits with width $w = 200$ nm were subsequently fabricated. They are located to the left (right) of the square nanoarrays, 10 μm (2 μm) away. A semiconductor laser ($\lambda = 655$ nm) was placed on top of the samples and the SPP waves were launched by the in-coupling slit. The optical images and scanning electron microscopy (SEM) images of the samples with different disorder degrees are shown in Figs. 4(b) and 4(c), respectively. When SPPs travel along with the silver layer, some of the SPP waves are localized around the nanohole units, after which the leaky modes are excited. In the experiments, we capture the leaky modes via an oil lens beneath the samples [see Fig. 4(a)]; thus, the collected leaky modes are mainly from the SPPs at the Ag–glass interface. Figure 4(d) shows the captured images from the charge-coupled-device (CCD) camera for $\eta = 0\%$–60%, where the power of the laser is maintained for all conditions. The field distribution gradually shrinks and is localized near the SPP launch spot, with an increasing disorder degree. To show quantitatively the distinctions among the field distributions in different nanostructures, we plot the experimental field intensity profiles across the brightest spot of leaky modes along both the x-direction [to see Fig. 4(e)] and the y-direction [to see Fig. 4(f)] in the samples with the disorder degrees from 0% to 60%. The main intensity peak of the collected signal in the disordered structure ($\eta = 60\%$) is more than twice larger than that in periodic structure ($\eta = 0\%$). This agrees with the simulations. The experimentally derived inverse participation ratio P and effective propagation length L_{eff} of SPPs are shown in Fig. 4(g), exhibiting similar tendencies to the calculation results discussed above. Besides, the out-coupling slit, located at the end of the square nanoarrays, can couple to the in-plane SPPs and radiate light to free space. As shown in Fig. 4(d), the signal from the out-coupling slit is remarkably reduced as the disorder degree increases. The integrated intensity as a function of the disorder degree is plotted in Fig. 4(h). It exponentially decreases with the disorder degree. These experimental observations imply that the SPPs are indeed trapped in the disordered nanoarrays.

Furthermore, we explore the influence of 2D Anderson localization on SPP-exciton interactions. Here, excitons are introduced by combining dye molecules with our 2D disordered nanohole arrays. We chose an infrared fluorescent dye molecule (IR-140, Sigma-Aldrich) with a PL resonance at approximately 850 nm, to avoid overlapping with the laser wavelength. The IR-140 dye was dissolved in the anisole and then spin-coated on top of the fabricated samples. The optical images of the samples, with and without the spin-coated IR-140 dye, are displayed in Fig. 5(a). We can see the color contrast after the sample is coated with the IR-140 dye. Owing to the SPP-exciton energy transfer, the dye molecules can interact with the near-field plasmonic waves along the silver surface and consequently form dye PL emitters. The PL images are directly captured using an electron-multiplying CCD (EMCCD) camera with light filters. Figures 5(b) and 5(c) show the PL images of periodic ($\eta = 0\%$) and disordered ($\eta = 60\%$) nanohole arrays coated with IR-140 dye, under excitation with laser wavelength $\lambda = 655$ nm. The PL signal from the periodic nanohole array with dye molecules is distributed weakly across the

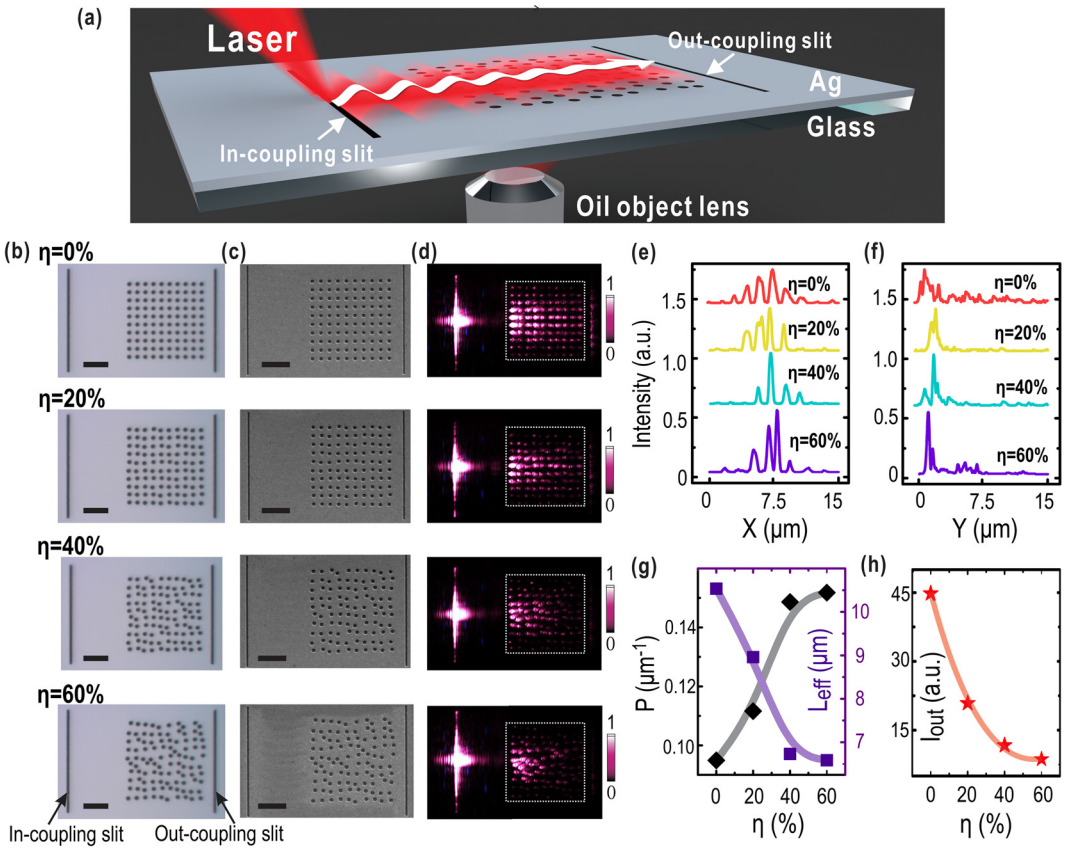

FIG. 4. (a) Schematic of the experimental setup. The incident laser is coupled to the silver surface through the in-coupling slit. The leaky modes are collected by an oil object lens placed beneath the fabricated samples. (b) and (c) Optical and SEM images of the samples with increasing disorder degree from $\eta = 0\%$ to $\eta = 60\%$, respectively. Each scale bar is 5 μm. (d) CCD-captured leaky mode images of the samples with different disorder degree corresponding to (a) and (b). Each subplot is at the same scaling. At each subplot, the white dashed square denotes the patterned area with nanoholes, which has 15 μm in the vertical *x*-direction and 15 μm in the horizontal *y*-direction. (e) and (f) The CCD-captured field intensity profile across the brightest spot of leaky mode along the *x*-direction (e) and along the *y*-direction (f) in the samples with the disorder degree from 0% to 60%, respectively. Each subplot is plotted at the same scaling. (g) Experimental inverse participation ratio and effective propagation length as a function of disorder degree. (h) Experimental integrated field intensities of the out-coupling slit as a function of disorder degree.

entire structure. However, in the disordered nanostructure ($\eta = 60\%$) with dye molecules, the PL signal is spatially localized to the left-center of the square array. As shown in the experimental PL intensity profiles across the strongest spot along the *x*-direction [to see Fig. 5(d)] and along the *y*-direction [to see Fig. 5(e)] in two samples, we can find that the PL signal from the IR-140 dye on the disordered nanohole array is highly enhanced. Compared to the IR-140 dye on the periodic nanohole array, the maximum of the PL intensity has been increased by approximately one order of magnitude. Compared to the IR-140 dye on the flat silver film without nanostructures [i.e., the unpatterned area in Figs. 5(b) and 5(c)], however, the PL signal can be enhanced by over three orders of magnitude. These PL signal enhancements originate from the SPP-exciton coupling between the nanostructures and IR-140 dye. Here, the SPPs are excited not only at the Ag–glass interface but also at the Ag–dye interface, both of which may contribute together to the interaction with the excitons. Physically, in the periodic nanostructure, there exists SPP-induced light confinement; however, in the disordered nanostructure, Anderson localization of SPPs associates spatial-disorder-induced light localization with SPP-induced light confinement, and thus makes stronger field confinement and enhances the light–matter interaction.

In conclusion, we have demonstrated the Anderson localization of SPPs in 2D disordered systems in the visible regime. By introducing short-range positional disorder in the 2D nanohole arrays, Anderson localization of SPPs occurs and is quantitatively verified by the exponentially decreased electric fields, the reduced effective propagation length, and the rapid disappearance of the autocorrelation coefficient. Fourier transformation of the calculated electric-field distributions shows that the strong localization originates from multiple scattering among the disordered local units within the nanostructures. Furthermore, we realize the localized SPP-exciton interactions in the 2D disordered nanoarrays combined with fluorescent dye molecules, and the photoluminescence signal from fluorescent dye molecules has been enhanced by over three orders of magnitude compared to that on the silver film without nanostructures. Our results constitute a significant step toward 2D Anderson localization of SPPs in a visible regime and offer a unique platform to effectively control the light–matter interactions.

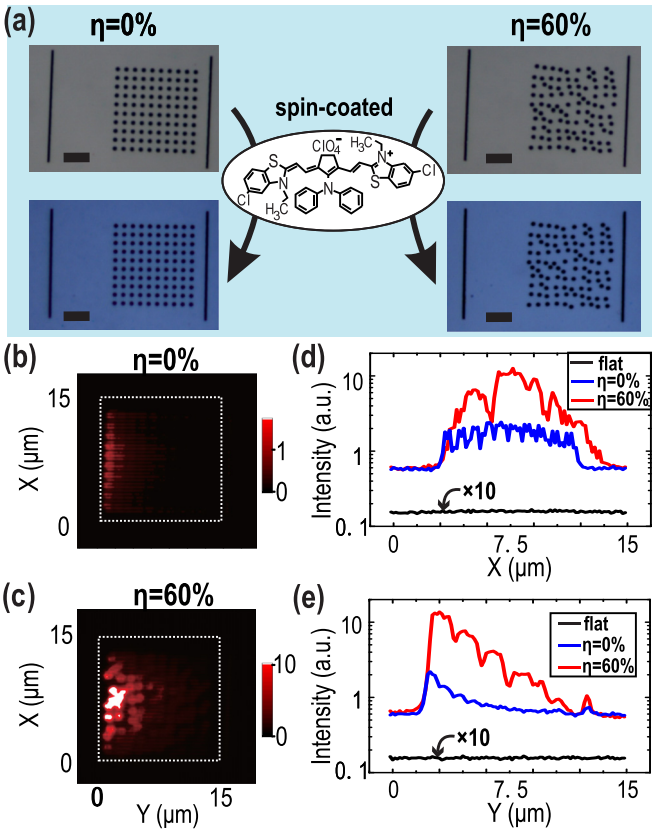

FIG. 5. (a) Optical images of the 2D nanohole arrays with disorder degrees of 0% and 60%. The top (bottom) set of images are of the samples without (with) the spin-coated IR-140 dye. Each scale bar is 5 μm. The chemical formula of IR-140 is included. EMCCD-captured PL images of the spin-coated samples with disorder degree (b) 0% and (c) 60%, respectively. In each sample, the IR-140 dye layer is covered on both the patterned area with nanoholes (within the white dashed square) and the unpatterned flat area without any nanoholes (outsides of the white dashed square). (d) and (e) Experimental PL intensity profile across the strongest spot along the *x*-direction (d) and along the *y*-direction (e) in two samples, where blue and red curves are the PL signals from the spin-coated samples with disorder degrees of 0% and 60%, respectively. Besides, black curves in (d) and (e) show tenfold of the PL signals from the IR-140 on the flat silver film without nanoholes.

This work was supported by the National Key R&D Program of China (No. 2017YFA0303702) and the National Natural Science Foundation of China (Grant Nos. 11634005, 11974177, 61975078, and 11674155).

The authors declare no conflicts of interest.

DATA AVAILABILITY

The data that support the findings of this study are available from the corresponding authors upon reasonable request.

REFERENCES

[1]P. Berini and I. D. Leon, Nat. Photonics **6**, 16 (2012).
[2]M. Aeschlimann, T. Brixner, D. Differt, U. Heinzmann, M. Hensen, C. Kramer, F. Lükermann, P. Melchior, W. Pfeiffer, and M. Piecuch, Nat. Photonics **9**, 663 (2015).
[3]A. V. Zayats, J. Elliott, I. I. Smolyaninov, and C. C. Davis, Appl. Phys. Lett. **86**, 151114 (2005).
[4]D. Pan, H. Wei, L. Gao, and H. Xu, Phys. Rev. Lett. **117**, 166803 (2016).
[5]T. J. Echtermeyer, S. Milana, U. Sassi, A. Eiden, M. Wu, E. Lidorikis, and A. C. Ferrari, Nano Lett. **16**, 8 (2016).
[6]P. Berini, Laser Photonics Rev. **8**, 197 (2014).
[7]P. L. Stiles, J. A. Dieringer, N. C. Shah, and R. P. V. Duyne, Annu. Rev. Anal. Chem. **1**, 601 (2008).
[8]W. Zhu, T. Xu, H. Wang, C. Zhang, P. B. Deotare, A. Agrawal, and H. J. Lezec, Sci. Adv. **3**, e1700909 (2017).
[9]E. K. Keshmarzi, R. N. Tait, and P. Berini, Nanoscale **10**, 5914 (2018).
[10]E. K. Tanyi, S. Mashhadi, C. On, M. O. Faruk, E. Harrison, N. Noginova, and M. A. Noginov, Appl. Phys. Lett. **115**, 151103 (2019).
[11]Z. Zhang, Y. Fang, W. Wang, L. Chen, and M. Sun, Adv. Sci. **3**, 1500215 (2016).
[12]H. C. Zhang, Y. Fan, J. Guo, X. Fu, and T. J. Cui, ACS Photonics **3**, 139 (2016).
[13]M. Hu, L. Yang, H. Dai, and S. He, Sci. Rep. **7**, 4809 (2017).
[14]E. Ozbay, Science **311**, 189 (2006).
[15]Q. Hu, D.-H. Xu, Y. Zhou, R.-W. Peng, R.-H. Fan, N. X. Fang, Q.-J. Wang, X.-R. Huang, and M. Wang, Sci. Rep. **3**, 3095 (2013).
[16]Z. Shao, Y. Yang, Z. Wang, M. Yahaya, B. Zheng, S. Dehdashti, H. Wang, and H. Chen, Opt. Express **25**, 10515 (2017).
[17]S. Vivekchand, C. J. Engel, S. M. Lubin, M. G. Blaber, W. Zhou, J. Y. Suh, G. C. Schatz, and T. W. Odom, Nano Lett. **12**, 4324 (2012).
[18]J. Chen, M. Badioli, P. Alonso-González, S. Thongrattanasiri, F. Huth, J. Osmond, M. Spasenović, A. Centeno, A. Pesquera, and P. Godignon, Nature **487**, 77 (2012).
[19]Y. Bao, S. Zu, Y. Zhang, and Z. Fang, ACS Photonics **2**, 1135 (2015).
[20]M. Segev, Y. Silberberg, and D. N. Christodoulides, Nat. Photonics **7**, 197 (2013).
[21]D. S. Wiersma, Nat. Photonics **7**, 188 (2013).
[22]F. Riboli, N. Caselli, S. Vignolini, F. Intonti, K. Vynck, P. Barthelemy, A. Gerardino, L. Balet, L. H. Li, and A. Fiore, Nat. Mater. **13**, 720 (2014).
[23]M. Mascheck, S. Schmidt, M. Silies, T. Yatsui, K. Kitamura, M. Ohtsu, D. Leipold, E. Runge, and C. Lienau, Nat. Photonics **6**, 293 (2012).
[24]P. Hsieh, C. Chung, J. McMillan, M. Tsai, M. Lu, N. Panoiu, and C. W. Wong, Nat. Phys. **11**, 268 (2015).
[25]Z. Zhao, F. Gao, R. Peng, L. Cao, D. Li, Z. Wang, X. Hao, M. Wang, and C. Ferrari, Phys. Rev. B **75**, 165117 (2007).
[26]T. Schwartz, G. Bartal, S. Fishman, and M. Segev, Nature **446**, 52 (2007).
[27]Y. Lahini, A. Avidan, F. Pozzi, M. Sorel, R. Morandotti, D. N. Christodoulides, and Y. Silberberg, Phys. Rev. Lett. **100**, 013906 (2008).
[28]L. Levi, Y. Krivolapov, S. Fishman, and M. Segev, Nat. Phys. **8**, 912 (2012).
[29]N. A. Wasley, I. J. Luxmoore, R. J. Coles, E. Clarke, A. M. Fox, and M. S. Skolnick, Appl. Phys. Lett. **101**, 051116 (2012).
[30]J. Topolancik, B. Ilic, and F. Vollmer, Phys. Rev. Lett. **99**, 253901 (2007).
[31]L. Martin, G. Di Giuseppe, A. Perez-Leija, R. Keil, F. Dreisow, M. Heinrich, S. Nolte, A. Szameit, A. F. Abouraddy, and D. N. Christodoulides, Opt. Express **19**, 13636 (2011).
[32]S. Karbasi, R. J. Frazier, K. W. Koch, T. Hawkins, J. Ballato, and A. Mafi, Nat. Commun. **5**, 3362 (2014).
[33]J. Liu, P. D. Garcia, S. Ek, N. Gregersen, T. Suhr, M. Schubert, J. Mork, S. Stobbe, and P. Lodahl, Nat. Nanotechnol. **9**, 285 (2014).
[34]D. S. Wiersma, Nat. Phys. **4**, 359 (2008).
[35]R.-H. Fan, B. Xiong, R.-W. Peng, and M. Wang, Adv. Mater. 1904646 (2019).
[36]W.-B. Shi, L.-Z. Liu, R. Peng, D.-H. Xu, K. Zhang, H. Jing, R.-H. Fan, X.-R. Huang, Q.-J. Wang, and M. Wang, Nano Lett. **18**, 1896 (2018).
[37]D. Jović and C. Denz, Phys. Scr. **T149**, 014042 (2012).
[38]Y. Inose, M. Sakai, K. Ema, A. Kikuchi, K. Kishino, and T. Ohtsuki, Phys. Rev. B **82**, 205328 (2010).
[39]Y. Nishijima, L. Rosa, and S. Juodkazis, Opt. Express **20**, 11466 (2012).
[40]N. L. Thomas, R. Houdré, D. Beggs, and T. Krauss, Phys. Rev. B **79**, 033305 (2009).